Computers and Mathematics with Applications 78 (2019) 2407–2416

Contents lists available at ScienceDirect

Computers and Mathematics with Applications

journal homepage: www.elsevier.com/locate/camwa

Validation of Mechanical Layer Equivalent Method for simulation of residual stresses in additive manufactured components

Marvin Siewert [a,*], Fabian Neugebauer [a,1], Jérémy Epp [b], Vasily Ploshikhin [a]

[a] ISEMP Institute, Department of Physics, University Bremen, Germany
[b] Leibniz-Institut für Werkstofforientierte Technologien, University Bremen, Germany

ARTICLE INFO

Article history:
Received 31 January 2018
Received in revised form 15 July 2018
Accepted 6 August 2018
Available online 9 October 2018

Keywords:
Additive manufacturing
Simulation
Mechanical layer equivalent method
Residual stress
Experimental validation
X-ray measurement

ABSTRACT

A challenge in the additive manufacturing process of laser beam melting of metals is the formation of residual stresses, which can cause large part deformations, when the part is released, lower the application range concerning tensile loads and provoke cracks. Due to the complexity and the interaction of different process parameters, the use of experimental studies for investigation is tedious and costly. An effective approach to analyze the effects is the numerical process simulation based on the method of finite elements. In this paper, the recently developed method of Mechanical Layer Equivalent for fast calculations of process induced distortions in laser beam melting is used to analyze the residual stresses during laser beam melting. For this purpose, small test samples have been generated additively and residual stresses have been measured by X-ray diffraction and compared to simulated values. The results show that despite the simplifications the model inhibits reliable prediction of residual stresses can be achieved.

1. Introduction

The technology of additive manufacturing enables the generation of complex three dimensional parts in a layer-based manner from CAD-data. For the manufacturing of metallic parts, the powder based process of selective laser beam melting (LBM) has established and gains more and more importance in the field of rapid manufacturing [1]. A detailed overview of powder based additive manufacturing processes can be found in [2]. In these processes iteratively thin layers of powder are spread by a roller and exposed by a laser beam following a pre-defined trajectory (scanning strategy). By heat diffusion the molten layers consolidate. After exposure of a layer the base plate of the build chamber lowers and the next layer of powder is applied. The repetition of these steps generates the parts. Thin support structures may be used to support the mechanical fixation onto the build plate. As laser beam melting can be considered as a series of micro-welding processes, it challenges the same problems in the context of residual stresses and deformations like conventional welding [2,3]. When new powder is applied on top of the part, a strong temperature gradient develops due to the rapid heating of the uppermost layer. After the exposure, its thermal shrinkage is hindered because of the underlying already solidified material. In consequence high residual stresses arise. After the process, when the components are released from the base plate, a new mechanical steady state is reached and the part deforms according to this. Recently, the method of numerical process simulation has

* Corresponding author.
E-mail address: siewert@isemp.de (M. Siewert).

[1] Meanwhile moved to Materialise GmbH, Mary-Somerville-Str. 3, Bremen, Germany.

https://doi.org/10.1016/j.camwa.2018.08.016
0898-1221/

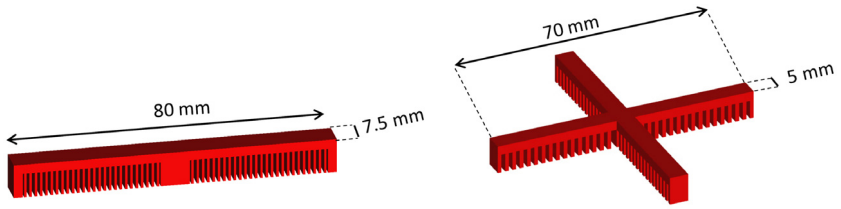

Fig. 1. Geometry of cantilever samples. Twin-cantilever (left) and Cross-cantilever (right).

become an important and powerful tool to predict residual stress and distortion in thermal manufacturing processes. Due to the complexity of the process and the interacting orders of effects, the thermomechanical simulation of the full process is not applicable [4]. Instead, several approaches for simplification have been developed. By taking such simplifications into account it was possible to realize different thermomechanical simulation methods in the past, e.g. [4–9].

Therefore the summary of several process layers to a single finite element layer [4–6] has been used. Zaeh and Branner [6] charged these layers with a constant thermal load for a short time interval as heat input in their thermomechanical approach. A discussion about the effects of simplifying the heat source from detailed hatches to distributed heat input on small regions or even full layers can be found in [10]. Further approaches are the condensation of scan paths [7] and the geometry dependent assignment of a surface heat input according to an analysis of filigree [11].

As the validation of those methods is easier comparing macroscopic part deformations, the larger number of published work focuses this, e.g. Neugebauer et al. [7] obtained good accordance of the measured part distortion of generated cantilevers of Steel X4CrNiCuNb 16-4 when the scan paths where condensed.

In order to achieve fast calculation of part distortion, the method of the Mechanical Layer Equivalent (MLE) has been developed [12,13]. It is based on the inherent strain method known from welding simulations [14,15]. It dramatically reduces the calculation time compared to classical thermomechanical approaches and is therefore well suitable for application in an industrial environment, where e.g. design engineers need a fast estimation of deformation and residual stresses which occur during the buildup of their designed parts. The method has been proven to be successful in terms of prediction of part distortion as well as to minimize them by using its results for a simulation based pre-deformation.

Aim of this paper is to investigate the quality of the method of Mechanical Layer Equivalent on the prediction of residual stresses. For this purpose, several samples have been generated from Ti6Al4V. The residual stress was measured by X-ray diffraction and compared to simulated values.

2. Methods and experiments

2.1. Samples and their manufacturing parameters

For experimental investigation of residual stresses and part distortion, cubic samples with a ground section of 10 × 10 mm^2 and varying height of 10 and 20 mm resp. has been build up. Furthermore Twin- as well as Cross-cantilevers samples were generated (Twin- and Cross-cantilever geometries are shown in Fig. 1). All samples were generated from Ti6Al4V on a M2 cusing machine by Concept Laser GmbH.

After the process, the parts were cut from the base plate by milling. In order to compensate the amount of material which gets lots during the cut off, 5 mm in height were added to all samples at the bottom sides by the manufacturer. In the milling process, the undermost 3.5 mm of the parts were removed.

Two different types of the scan strategy were used for the cubic samples, namely (a) "bilinear" and (b) "bilinear" with a rotation of 90° between consecutive layers (Fig. 2). In case of the Twin-cantilevers two types of bilinear scanning were used, namely 'bilinear long' for those parts which where exposed parallel to the long side and 'bilinear short' for those with scanning parallel to the short side, i.e. orientation of scan vectors is not changed after each layer in case of Twin-cantilevers. The Cross-cantilever geometries were also scanned bilinear. Here all scan vectors are parallel, so that one lever of the Cross-cantilever is scanned similar to bilinear long and the other lever similar to bilinear short. The scan strategies are illustrated schematically in Fig. 3. After the fill scan, the contour was scanned additionally.

2.2. Distortion measurement

Distortions of the cantilevers were measured using a VR-3000 Macroscope by Keyence. As 'z-displacement' the distance of the part's middle point on the surface to a line, given by two points on the bended edges of the parts, was used. To compare Cross-cantilever distortions with simulation results the z-displacements were measured on the two main paths of the Cross-cantilever, i.e. one path parallel (*Path 1*) and one orthogonal (*Path 2*) to the used scan vectors. The paths are illustrated in Fig. 4.

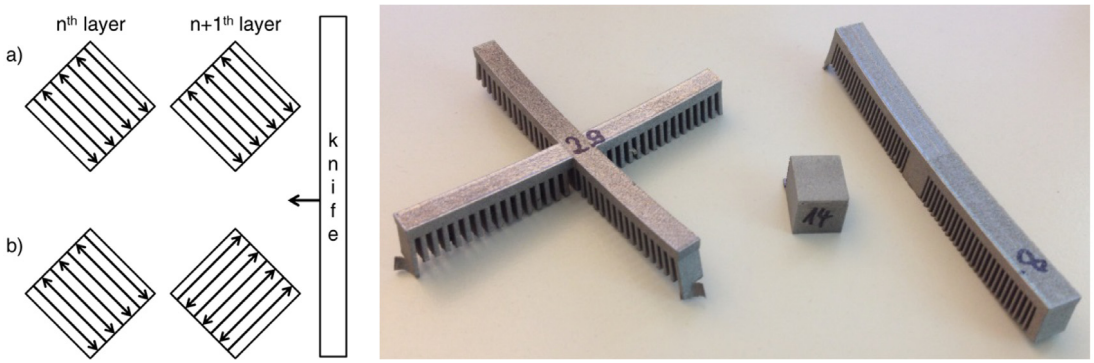

Fig. 2. Used scan strategies for cubic samples (left) and generated samples (right).

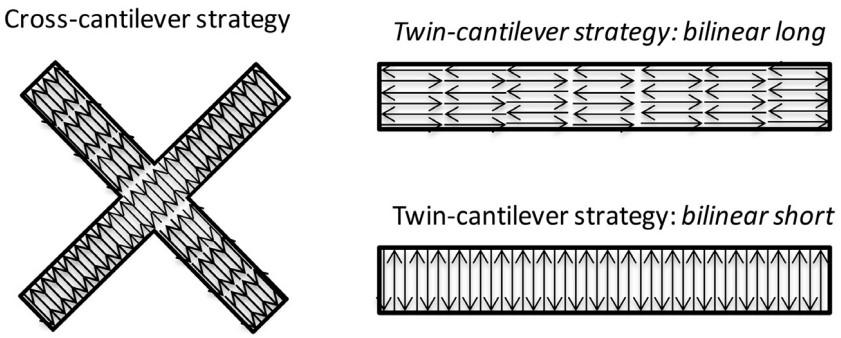

Fig. 3. Used scan strategies for Cross-cantilever samples (left) and Twin-cantilever samples (right).

Fig. 4. Measurement of Twin-cantilever distortion (left) and path for Cross-cantilever measurements (right).

2.3. Residual stress measurement

The X-ray diffraction measurements were performed with a Bruker-AXS D8 diffractometer using Cu-Kα radiation. The detector was a scintillation counter with a Ni-Filter in order to remove the Kβ-radiation. The residual stress measurements were performed at the {213} peak of α-Ti at $2\Theta = 141°$ with 15 different χ-tilt angles between $-45°$ and $45°$. The samples were measured at different surfaces (x, y, z) in different directions in order to determine the different stress components σ_{11}, σ_{22} and σ_{33}. Fig. 5 shows a top view of a sample with the defined coordinate system, regarding the direction marker present on each sample. The beam diameter was 2.4 mm and was placed in the center of the measured surface, as shown in Fig. 5. The evaluation of the measurements was performed using the standard $\sin^2 \Psi$ method after linear background subtraction and determination of the peak position by the center of gravity method [16]. With this method, the residual stresses are determined based on linear regression and determination of the mean slope of the peak position evolution over $\sin^2 \Psi$ while the error is related to the regression coefficient. The X-ray elastic constant $\frac{1}{2}S_2 = 1.16 \times 10^{-5}\,\mathrm{MPa}^{-1}$ has been used to calculate the residual stresses.

In order to measure residual stress depth profiles, the surface of the samples was removed progressively by electrochemical etching and measured by X-ray diffraction method again. The electrochemical etching has been executed using a hydrogen-peroxide solution at the complete investigated surface. Of course material removal at the considered surfaces influences the stress state in a sample. Therefore the measured stresses correspond to stress states after material removal and differ from stresses in the inside of (unchanged) specimen after cut off from the base plate. In order to compare measured and computed results the material abrasion has to be included in the simulations. More details about how this is done can be found at the end of the corresponding Section 2.5.

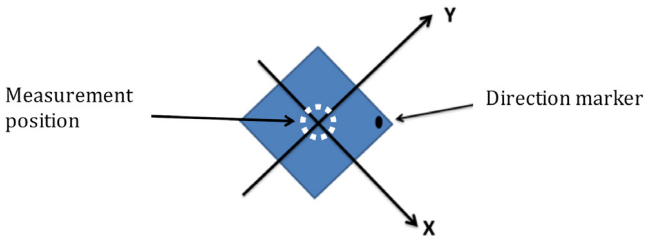

Fig. 5. Top view of a sample with the defined coordinate system.

2.4. Classical thermomechanical approach for process simulations

To describe the occurring deformation and residual stresses in a suitable continuums mechanical framework let $u : \Omega \to \mathbb{R}^3$ denote the displacement vector field defined on an open bounded domain $\Omega \subset \mathbb{R}^3$ with sufficiently smooth boundary, which represents the specimens geometry. As usual in engineering science the considered strain tensor is defined by $\varepsilon = \frac{Du+Du^T}{2}$ with its decomposition $\varepsilon = \varepsilon^{\text{el}} + \varepsilon^{\text{pl}} + \varepsilon^{\text{th}}$ into elastic-, plastic- and thermal strains.

A natural approach to simulate the process is to solve heat conductivity equation

$$c\partial_t T + \nabla \cdot (\kappa \nabla T) = q,$$

where T is the temperature and c, κ are heat capacity and heat conductivity, respectively. For this purpose suitable initial and boundary conditions have to be defined as well as the heat source q, which represents the absorption of the laser energy. The solution has to be computed for the whole process time and its spatial domain is the growing part together with the surrounding powder. The surrounding powder is often neglected to save computational time, since its heat conductivity is much smaller compared to solid material. The computed temperature field defines the occurring thermal strains

$$\varepsilon^{\text{th}} = \int_0^t \alpha(T)\text{ds} \begin{bmatrix} 1 & 0 & 0 \\ 0 & 1 & 0 \\ 0 & 0 & 1 \end{bmatrix},$$

depending on the coefficient of thermal expansion α. The thermal strains can be taken into account to compute static mechanical equilibrium, i.e.

$$\nabla \cdot \sigma = 0. \tag{1}$$

According to Hook's law the stress tensor σ depends linear on $\varepsilon^{\text{el}} = \varepsilon - \varepsilon^{\text{pl}} - \varepsilon^{\text{th}}$ and the evolution of the strain components ε^{el}, ε^{pl} is determined by a suitable material model containing flow-conditions and -rules, e.g. associated perfect plasticity with von Mises flow rule [17].

2.5. Difficulties of the thermomechanical simulation approach and the MLE method

Although modern methods like the Finite Element Method (FEM) (cf. [18,19] for a discussion from a mathematical or [20] from an engineering point of view) make it possible to solve these equations approximately the computation effort is quite high. Note that in laser beam melting processes typically high temperature gradients occur, which imply the need of many time steps in the computation of the temperature field. Small regions near to the laser spot exhibits temperatures above liquidus temperature, whereas the bulk of the part is much cooler. Thermal strains stemming from heat up and cool down phases in hot regions surrounded by cold and stiff material causes a high rate of plastic deformations. In order to gain appropriate accuracy it is necessary to consider the load history correctly, i.e. mechanical equilibrium has to be solved for many time steps, too.

Additionally the calibration and validation of the computed temperatures is nearly impossible. Temperature measurements during the process anywhere inside the build chamber are costly and restricted to small regions of the part, e.g. the surface of the uppermost layer in case of thermographic cameras or to the base plate in case of thermal elements. This together with the high computational effort makes this natural approach unattractive and impossible for process simulation of large parts, e.g. most industrial relevant parts.

To overcome these problems, Keller developed the MLE method [12,13]. MLE is based on the inherent strain method known from welding simulations. In welding processes, all points near the weld path have similar temperature histories and therefore develop approximately the same strains remaining in the path. This motivates the inherent strain methods, where not the full thermomechanical computation is executed. Instead the inherent strains $\varepsilon^* = \varepsilon^{\text{pl}} + \varepsilon^{\text{th}}$, i.e. the sum of plastic and thermal strain at end of the process, are inserted as loads in only one computation of mechanical equilibrium. This gives the distortion and residual stresses at the end of welding processes.

To identify the inherent strains for the simulation of long weld paths, one can simulate only a short part of the weld path and postulate that the occurring inherent strains will not change significantly even if the weld path will be longer.

Table 1
Laser parameters used for the build up of specimens.

Laser power (fill)	180 W
Laser power (contour)	180 W
Laser speed (contour)	1250 mm s^{-1}
Laser speed (fill)	1250 mm s^{-1}
Hatch distance	0.105 mm
Layer thickness	0.03 mm
Beam correction	0.03 mm

Table 2
Material parameters used for the simulations.

Poisson ratio	0.31
Young's modulus	110 GPa
Yield stress	1030 MPa

This is a legitimate simplification as long as the temperature history in the short weld path will be the same as in the long one and the local geometry near to the melt pool will not change significantly. In case of laser beam melting, Keller studied the development of inherent strains during the buildup of one island, i.e. a small rectangular region of a full part. The investigation was performed by thermomechanical FEM calculation as described above. He figured out that the occurring strains ε^*_{xx} and ε^*_{yy} which remain in the part are almost constant on that area, i.e. they only differ in very small regions near to the island boundary. Similar to the inherent strain calculations for long weld path simulations these inherent strains can be inserted as loads into a pure mechanical calculation to compute an approximation of distortions and residual stresses of even large LBM parts.

This approach results in the MLE method which is described by the following scheme: The specimen is discretized by a layer based FEM mesh. The FEM layers which usually consist of several process layers will be activated iteratively one after another. After activation each new layer is first set stress free and then mechanical equilibrium will be computed, where the inherent strains are inserted as loads in the new layer. The material behavior is described by associated perfect plasticity with von Mises flow rule. The displacement of the bottom nodes is set to zero as a Dirichlet boundary condition. The corresponding material coefficients were taken from JMatPro software (V 8.0.5) and are outlined in Table 2.

To identify the inherent strains, one can use simulations of small regions as already mentioned or alternatively calibrate them by means of measured deformation of build specimens, e.g. the deformation of Twin-cantilever geometries can be measured very precisely with marginal effort. The latter way was used here and is described more precisely in 3.2.

After the process simulation the cut-off from the base plate and the material abrasion have to be taken into account, since they influence the stress state substantially. The material abrasion was simulated by calculation of mechanical equilibrium (1) after deactivating elements of one side layer and holding the strains after the process and cut-off in the remaining part (these strains include inherent strains, which were applied as loads, and additional plastic strains occurring during macroscopic MLE process simulation). The deactivation and calculation of (1) is performed iteratively one side layer after another. Two corresponding meshes are illustrated in Fig. 6.

3. Results

3.1. Distortion of 'Twin-cantilever' samples

As illustrated in Fig. 7 the Twin-cantilever scanned along the long axis (i.e. scan strategy bilinear long) warped most (z-displacement of 4.1 mm). This is almost twice of the distortion of the parts scanned along the short side of the cantilever (i.e. scan strategy bilinear short with z-displacement of 2.3 mm).

3.2. Calibration of the simulation model

According to the cantilever distortion, strain values for the MLE method were determined by an iterative procedure. Therefore Newton's method in $\mathbb{R}^2$ was applied to find the strain components ε^*_{xx} and ε^*_{yy} whereas the difference of the measured and computed cantilever distortion is zero.

Here both scan strategies bilinear long and bilinear short are taken into account. The MLE build up simulation of Twin-Cantilever samples with the (unknown) inherent strain tensor should reproduce the distortion corresponding to bilinear long strategy and after a 90° rotation of coordinates it should reproduce the distortions corresponding to bilinear short strategy.

The determined strains are $\varepsilon^*_{xx} = -0.47\%$ and $\varepsilon^*_{yy} = -0.20\%$. Shear strains were set to zero. The upper most layer is not fixed from above and therefore a non zero contribution of strain loads in build up direction will result in simple shrinkage of the new layer in build up direction, which in particular will not cause any force acting on the underlying part. The shrinkage of that layer itself will be neutralized/refilled with the build up/(stress free-)activation of the next layer. For this reason ε^*_{zz} can also be set to zero, since it has no effect on the computation. Note that this does not mean that during the simulation no

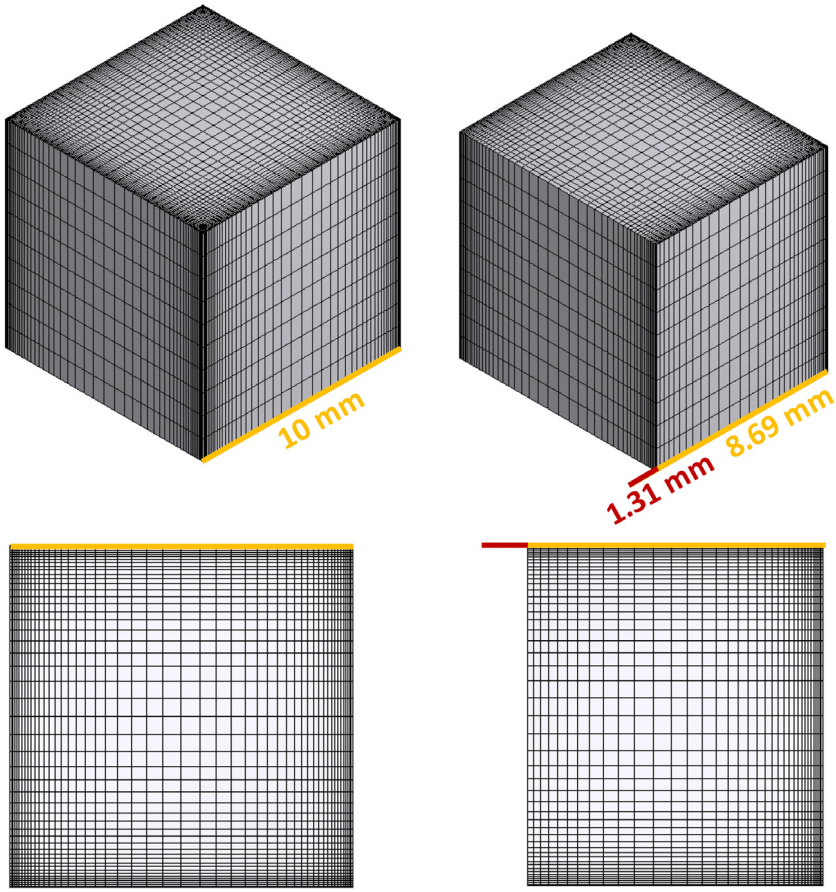

Fig. 6. Resulting meshes after element deactivation to simulate the material abrasion. No abraised material, i.e. no deactivated elements (left) and after 1.31 mm of removed material (right). Perspective view (top) and top view (bottom).

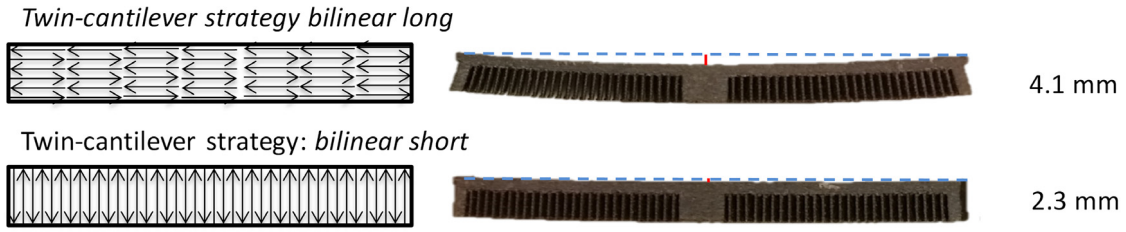

Fig. 7. Measured distortions of Twin-cantilevers, schematic illustration of scan vector orientation (left), corresponding deformation (right).

strain in build up direction will occur. Quite the contrary is the case since shrinkage in x and y direction of the uppermost layer can pull (segments of) the underlying part in build up direction. We will discuss that fact in Section 4 more detailed (e.g. Fig. 13)

As the calibrated values perfectly reproduced the Twin-cantilever distortion it is pointless to show the simulated and measured distortion here. However, the calibrated strains were used to simulate the distortion of the generated Cross-cantilevers as shown in Fig. 8. In the past MLE method has also been used successfully to simulate the distortion of more complex geometries, which in particular were very different compared to cantilevers [12].

To simulate the scan strategy with a rotation of 90° between consecutive layers the inherent strains are assumed to be equal in x and y direction, i.e. the mean values of ε^*_{xx} and ε^*_{yy} taken from the build up without layer rotation.

As described in Section 2.5 a model assumption of MLE method is that each new layer of a produced part develops the same inherent strains. Of course the shrinkage of every new layer will influence the strain and stress state of the underlying

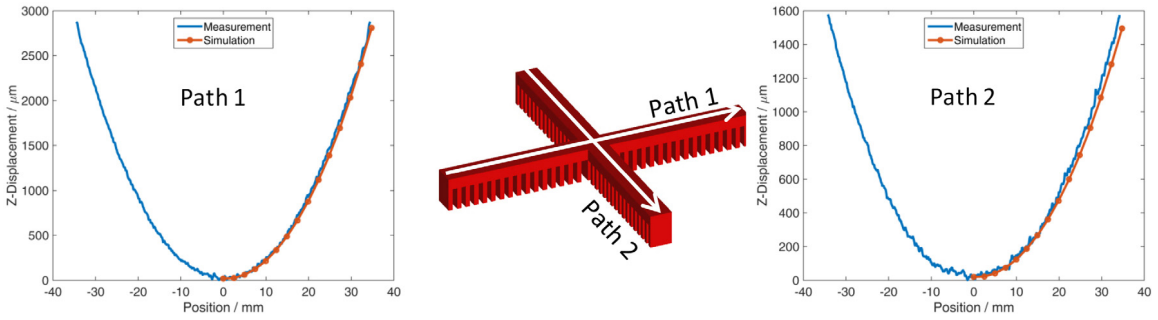

Fig. 8. Measured and simulated distortion of the Cross-cantilever. Path 1 parallel to scan vectors (left) and Path 2 orthogonal to scan vectors (right).

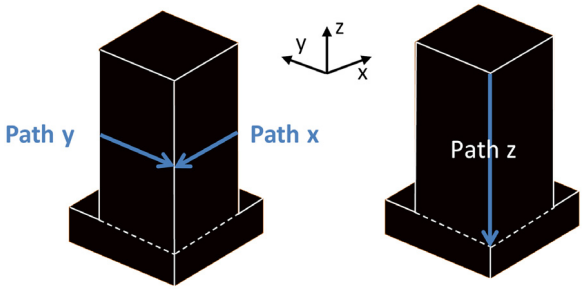

Fig. 9. Schematic illustration of the paths used for measurement and comparison with the simulations, Path/surface x and Path/surface y (left) and Path/surface z (right). Note that the Figure shows a quarter of the cubic sample.

part depending on its geometry and additional plastic deformation may occur. According to this, the identified inherent strains based on Twin-cantilever distortions can be used as loads in macroscopic MLE computations for any geometry of interest, e.g. for cubic samples as outlined in this paper. Note that inherent strains of course depend on the choice of process parameters (which were fixed here, cf. Table 1), i.e. a change of process parameters would entail a new calibration.

3.3. Residual stress simulation and comparison with measurements

In Figs. 10 to 12 the diagrams of the simulated stress values and the related measurements of the cubic samples are shown. In each diagram the surface name, which was used for etching and measurement, the stress component and the height of the cube are given. Three different paths were considered: Removal of material from the x–z-plane (surface/path y), from the y–z-plane (surface/path x) and from the x–y-plane (surface/path z). The x-axis is considered to be parallel to the scan vectors in case of bilinear scanning without layer rotation. All paths are passing in normal direction through the center of the respective plane. To allow comparison of simulated and measured data the paths used to analyze simulation data are of course the same paths which were used for measurements. A schematic illustration of the paths is given in 9. As already mentioned the measured and simulated stresses are obtained underneath the surface. Due to the material subtraction by etching, each time a new mechanical steady state is formed. In consequence the stress values given in the diagrams differ from the 'true stress' (i.e. stress of the non etched part) that would be measured using non-subtractive methods like neutron diffraction, which can measure stresses in the inner of parts.

4. Discussion

Although the simulation model is roughly simplified compared to the natural thermomechanical approach, the comparison of simulated and measured stresses shows good accordance in most cases. More precisely this holds true except for Fig. 10 surface x/σ_{zz}, Fig. 10 surface z/σ_{xx} and Fig. 10 surface z/σ_{yy}, whereas the last two cases reproduce at least roughly the right magnitude of the considered stress component. All other cases reproduce the development of stress curves in a high resolution. Note that due to limited resources some cases have less data points than others, so that e.g. Fig. 10 surface x/σ_{yy} has less significant information value compared to e.g. Fig. 10 surface y/σ_{zz}.

The stress measurements at surface x are subject to stronger variations than those of surface y (Fig. 10). This may be subjected to the scanning strategy causing a higher surface roughness at the surface of the x-path which is parallel to the laser paths. As the temperature in the laser reversal points is higher for longer times, more attachment of loose powder particles can occur. This may have an influence on the stresses and has not been considered in the simulation model.

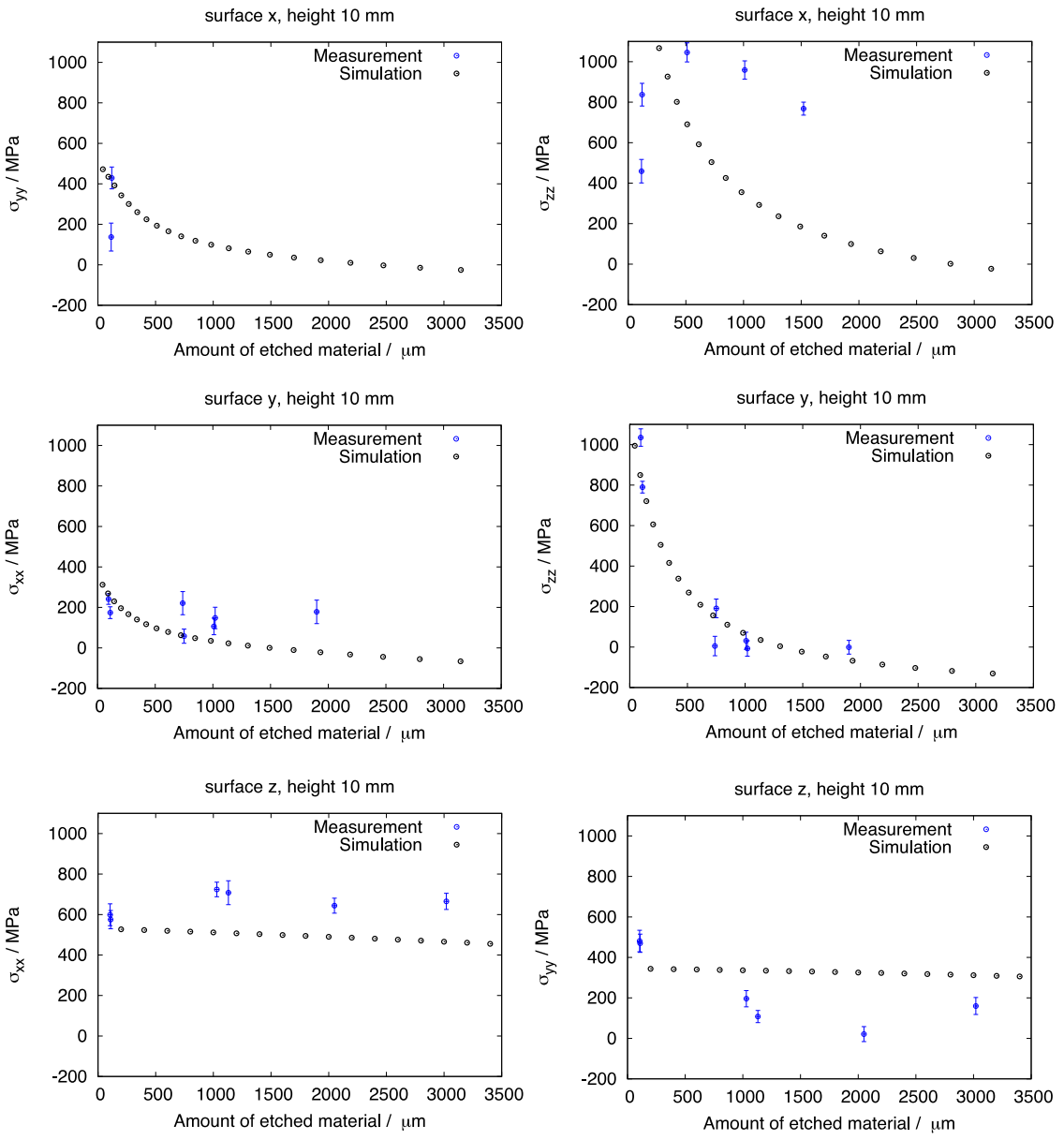

Fig. 10. Measured and simulated stresses of cube specimens with 10 mm height and no layer rotation scan strategy.

Regarding the rotated scan strategy, high accordance of simulation and measurement was achieved. As it is assumed in the model that the rotation of laser paths causes a homogenization of the strain field in x- and y-direction, simulated stresses σ_{xx} at y-surface and σ_{yy} at x-surface are equal. This assumption is confirmed by the measured data as the measured values are close in the range of overall scatter of the measurements as shown in 12.

Stress in build-up direction, i.e. σ_{zz} is highest at the surface. This is independent on the surface or the scanning strategy. The height of the part does not have a strong impact on the stress level of σ_{zz} at the surface, at least for the considered cubic parts. An explanation is given in Fig. 13: Due to the fixation to the base plate and the stiffness of the part itself, the underlying material below the cooling uppermost layer hinders a bending. In consequence high tensile stresses in build direction occur below the uppermost layer.

The calibrated inherent strains are anisotropic, i.e. the inherent strains in scan direction ε^*_{xx} are greater than the inherent strains ε^*_{yy} orthogonal to scan direction. This fits well to Kellers investigation concerning the development of inherent strains based on thermomechanical calculations. As one might expect, the use of such inherent strains yields to higher computed stress components in x-direction than in y-direction. The measurements confirm this fact (Fig. 10 surface z). To be more precise the difference between these stress components is even higher than forecasted by simulation.

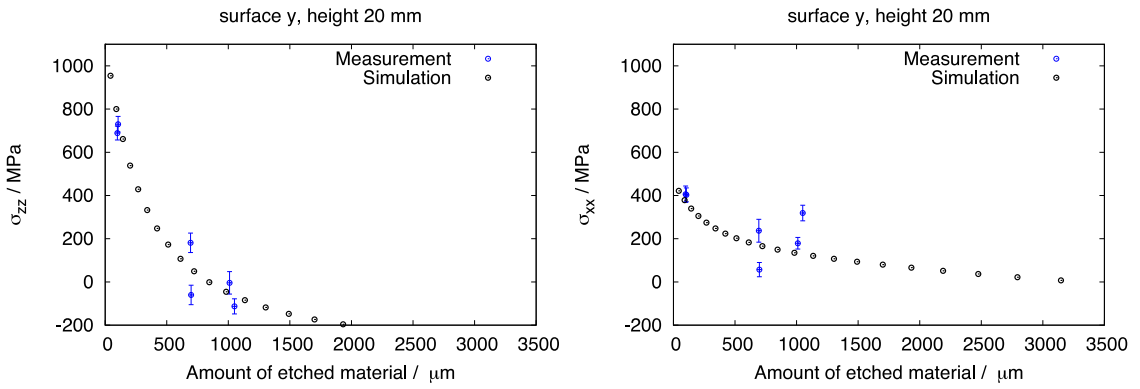

Fig. 11. Measured and simulated stresses of cube specimens with 20 mm height and no layer rotation scan strategy.

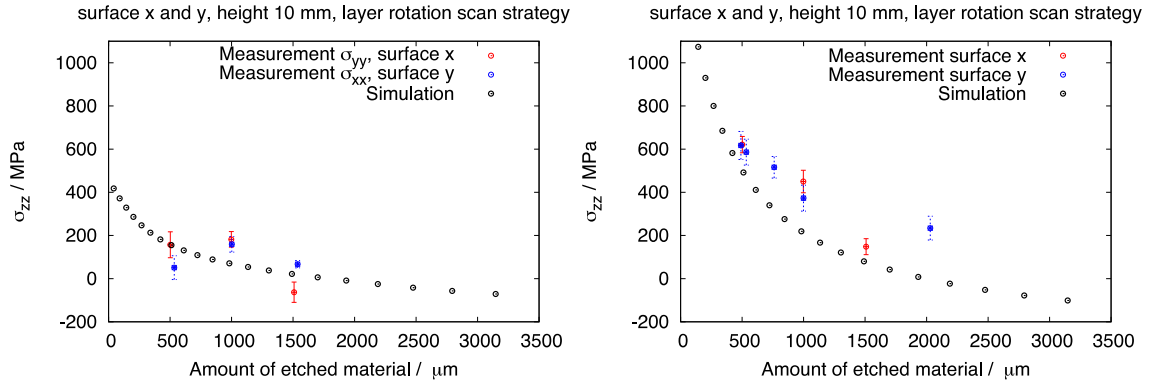

Fig. 12. Measured and simulated stresses of cube specimens with 10 mm height and layer rotation scan strategy.

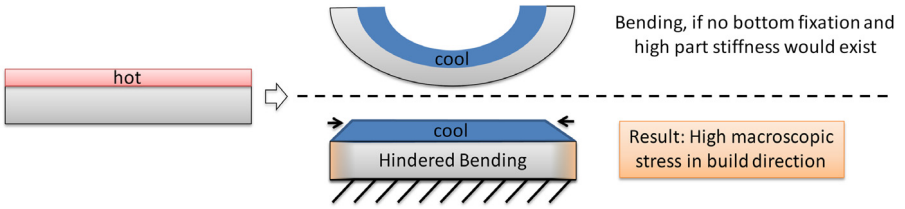

Fig. 13. Schematic explanation of the simulation model and the resulting tensile stresses in build up direction near to the surface.

Overall the results of the simulation show good accordance with the measurements and the method turns out as a suitable tool to get a fast estimation of distortions as well as residual stresses. In particular the critical areas with high tensile stress in build up direction close to the surface of the cubes has been identified very well.

Nevertheless, this work can only be understood as a first step in validating the MLE method, since only small specimens with simple geometry were analyzed. The method is based on the assumption that inherent strains will develop in a similar way in most regions of the part. In particular parts with a more complex geometry, overhanging regions and bigger parts should be analyzed as well, since regions on which the assumption is invalid will be greater in these cases.

Indeed we assume limitations of the method at its current state in these cases. It is well known that parts heat up during the process and therefore the thermal history in the first layers will be different compared to thermal history in the following layers. Up to a certain extend the resulting errors are small since the calibration will summarize the occurring inherent strains to a suitable mean value, but if the difference is too large one may have to adapt the method to consider different inherent strains. Furthermore the fact that parts will not cool down to room temperature will entail a change of material behavior and may cause additional macroscopic stresses, which are currently not taken into account by MLE method. Even though these stresses will vanish after the final cool down they might have an effect on the development of plasticity during the process, which will influence distortion and residual stresses remaining in the part even after cool down. To overcome this limitation it might be possible to include a fast thermal calculation based on e.g. a thermal layer activation and estimate the change of

occurring inherent strains depending on start and end temperature of each layer. Our suspected limitations as well as the approach to overcome them have to be checked carefully in further investigations.

5. Conclusion

In the presented study, the method of Mechanical Layer Equivalent (MLE) has been used to simulate the residual stresses in LBM fabricated Ti6Al4V samples. The residual stresses have been measured by X-ray diffraction and despite the strong simplifications the model is based on, good accordance of residual stress measurements and simulations was achieved in most cases. In particular the critical stresses have been reproduced by simulation very well.

Acknowledgments

These activities have been performed in the frame of the ALM ISCAR project managed by ArianeGroup GmbH funded within the ESA Future Launcher Preparatory Program (ESA FLPP).

References

[1] T. Wohlers, Wohlers Report 2018: 3D Printing and Additive Manufacturing State of the Industry : Annual Worldwide Progress Report, Wohlers Associates, 2018.
[2] S. Sun, M. Brandt, M. Easton, Powder bed fusion processes: An overview, in: M. Brandt (Ed.), Laser Additive Manufacturing, in: Woodhead Publishing Series in Electronic and Optical Materials, Woodhead Publishing, 2017, pp. 55–77, http://dx.doi.org/10.1016/B978-0-08-100433-3.00002-6.
[3] C. Li, Z. Liu, X. Fang, Y. Guo, Residual stress in metal additive manufacturing, Procedia CIRP 71 (2018) 348–353, http://dx.doi.org/10.1016/j.procir.2018.05.039, 4th CIRP Conference on Surface Integrity (CSI 2018).
[4] F. Neugebauer, N. Keller, H. Xu, C. Kober, V. Ploshkhin, Simulation of selective laser melting using process specific layer based meshing, in: A. Demmer (Ed.), Proceedings of the 2nd Fraunhofer Direct Digital Manufacturing Conference 2014 (DDMC 2014), Fraunhofer Verlag, Stuttgart, 2014, pp. 297–302.
[5] Y. Lee, W. Zhang, Mesoscopic simulation of heat transfer and fluid flow in laser powder bed additive manufacturing, in: Solid Freeform Fabrication Symposium, 2015, pp. 1154–1165–1237.
[6] M. Zaeh, G. Branner, Investigations on residual stresses and deformations in selective laser melting, Prod. Eng. 1 (2010) 35–45, http://dx.doi.org/10.1007/s11740-009-0192-y.
[7] F. Neugebauer, N. Keller, V. Ploshkhin, F. Feuerhahn, H. Koehler, Multi scale fem simulation for distortion calculation in additive manufacturing of hardening stainless steel, in: Int. Workshop on Thermal forming and welding distortion Proceedings, Bias-Verlag, 2014, pp. 13–23.
[8] L. Parry, I. Ashcroft, R. Wildman, Understanding the effect of laser scan strategy on residual stress in selective laser melting through thermo-mechanical simulation, Add. Manuf. 12 (2016) 1–15, http://dx.doi.org/10.1016/j.addma.2016.05.014.
[9] B.K. Panda, S. Sahoo, Numerical simulation of residual stress in laser based additive manufacturing process, IOP Conf. Ser.: Mat. Sci. Eng. 338 (1) (2018) 012030.
[10] C. Seidel, M. Zaeh, M. Wunderer, J. Weirather, T. Krol, M. Ott, Simulation of the laser beam melting process approaches for an efficient modelling of the beam-material interaction, 25 (2014) 146–153.
[11] N. Keller, F.N.H. Xu, V. Ploshikhin, Thermo-mechanical simulation of additive layer manufacturing of titanium aerospace structures, in: LightMAT Conference 2013 Proc., 2013.
[12] N. Keller, Verzugsminimierung bei selektiven laserschmelzverfahren durch multi-skalen-simulation (Ph.D. thesis), Bremen, 2017.
[13] N. Keller, New method for fast predictions of residual stress and distortion of am parts, in: Solid Freeform Fabrication Symposium, 2014, pp. 1229–1237.
[14] H. Ruiz, N. Osawa, H. Murakawa, S. Rashed, Prediction of distortion produced in welded structures during straightening process using the inherent strain method., http://dx.doi.org/10.1115/OMAE2016-54743.
[15] H. Murakawa, Y. Luo, Y. Ueda, Prediction of welding deformation and residual stress by elastic fem based on inherent strain, 1996 (1996) 739–751, http://dx.doi.org/10.2534/jjasnaoe1968.1996.180_739.
[16] J. Epp, X-ray diffraction rechniques for material characterization, in: G. Hbschen, I. Altpeter, R. Tschuncky, H.-G. Herrmann (Eds.), Materials Characterization Using Nondestructive Evaluation (NDE) Methods, Woodhead publishing, 2016, pp. 81–124.
[17] J.C. Simo, T.J.R. Hughes, Computational Inelasticity, Corr. 2. print ed., Interdisciplinary Applied Mathematics ; 7, Mechanics and Materials, Springer, New York, NY [u.a.], 2000, XIV, 392 S. : graph. Darst..
[18] D. Braess, Finite Elemente : Theorie, schnelle Loser und Anwendungen in der Elastizitatstheorie, fifth ed., in: Springer-Lehrbuch Masterclass, Springer, Berlin, 2013, Online-Ressource (XVI, 369 S.) : digital.
[19] S.H. Lui, Numerical Analysis of Partial Differential Equations, in: Pure and Applied Mathematics : A Wiley Series of Texts, Monographs, and Tracts, Wiley, Hoboken, N.J, 2011, http://dx.doi.org/10.1002/9781118111130, Online-Ressource (xiii, 487 p.) : ill.
[20] K.-J. Bathe, P. Zimmermann, Finite-Elemente-Methoden, second ed., Springer, Berlin [u.a.], 2002, XVI, 1253 S. : graph. Darst..